Energy 282 (2023) 128963

Contents lists available at ScienceDirect

Energy

journal homepage: www.elsevier.com/locate/energy

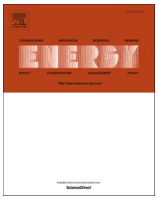

Thermodynamic and techno-economic analysis of a direct thermal oil vaporization solar power system

Pengcheng Li [a,c], Jing Ye [a], Jing Li [b,*], Yandong Wang [d], Xiaobin Jiang [a], Tongle Qian [a], Gang Pei [e], Xunfen Liu [a]

[a] School of Automotive and Transportation Engineering, Hefei University of Technology, 193 Tunxi Road, Hefei, China
[b] Research Center for Sustainable Energy Technologies, Energy and Environment Institute, University of Hull, Hull, HU6 7RX, UK
[c] DONGFANG ELECTRIC Dongfang Boiler Group CO., LTD., 150 Huangjue Ping, Wuxing Street, Zigong, China
[d] Hefei General Machinery Research Institute, 888 Changjiang Road, Hefei, China
[e] Department of Thermal Science and Energy Engineering, University of Science and Technology of China, 96 Jinzhai Road, Hefei, China

ARTICLE INFO

Handling editor: G Iglesias

Keywords:
Solar thermal power generation
Subcritical steam rankine cycle
Thermal oil
Organic rankine cycle
Equivalent heat-to-power efficiency

ABSTRACT

A unique direct thermal oil vaporization solar power system employing cascade organic-steam Rankine cycle is proposed. The oil is a mixture of biphenyl and diphenyl oxide, and it is used for heat transfer, storage and power cycle fluid in the novel system. Stable electricity output and prolonged storage capacity can be facilitated. In the rated mode, the oil is vaporized at 390 °C in the collectors and drives a top turbine. The exhaust heat is used for preheating and evaporating water of the bottom cycle. Meanwhile, the hot oil in a high-temperature tank (HTT) superheats and reheats the generated steam. When the irradiation is insufficient, the heat released by the oil from the HTT to a low-temperature tank drives the bottom cycle. Fundamentals, thermodynamic performance and techno-economic feasibility are elaborated. The results indicate that, compared with the mainstream dual-tank solar power systems, the proposed system has a higher thermal efficiency with a lower water evaporation temperature (42.90% at 260 °C vs. 38.06% at 310 °C) and a larger temperature drop between the two tanks (121 °C vs. 100 °C). The equivalent payback time with respect to the top oil cycle is less than 3 years.

1. Introduction

Concentrated solar power (CSP) has attracted widespread attention in recent decades. Unlike solar photovoltaic technologies, heat storage enables solar thermal power to be dispatchable, self-sustainable and flexible. The installed power capacity of global CSP reached 6.59 GWe based on the data as of the end of 2019, and the parabolic trough collectors (PTCs) related plants account for above 70% [1,2].

Fig. 1 illustrates the most advanced demonstration and commercial PTC plant using thermal oil as a heat transfer fluid and molten salts as a storage fluid [3,4]. The typical synthetic oil is a mixture consisting of 73.5% diphenyl oxide and 26.5% biphenyl, which possesses extraordinarily low viscosity and high stability in a large temperature interval from 12 °C to 400 °C. Its thermal stability is the highest among general organic heat carriers. Some key thermophysical parameters are provided in Table 1 [5].

However, synthetic oil is mainly used for the liquid phase heat transfer medium in existing CSP systems. The oil temperature increases from 290 °C at the solar field inlet to 390 °C at the outlet. The exergy of the oil will be exploited more efficiently if it is vaporized in the collectors. The efficient heat transfer coefficient and constant temperature in the two-phase region are beneficial to improve the solar field efficiency. Many organic Rankine cycle (ORC) working fluids have been studied in direct vapor generation (DVG) applications [6–14]. DVG can avoid secondary heat transfer and reduce irreversible loss as compared with an indirect configuration. As there is no need to superheat the ORC fluids, the sophisticated control strategies for the conventional direct steam generation (DSG) systems due to the requirement of superheated steam in the solar field are alleviated [6]. High-pressure (4–10 MPa) steam generation is replaced by organic vapor generation at relatively low pressure. Besides, the technical barriers accompanied by wet steam turbines are avoided by more efficient, dry ORC turbines [15]. However, only refrigerants, hydrocarbons and siloxanes are considered in the DVG systems and the fluid evaporation temperature is relatively low (<300 °C). Biphenyl-diphenyl oxide (BDO) mixture, which is suitable for the high-temperature application, has not been discussed or studied

* Corresponding author.
E-mail address: Jing.Li@Hull.ac.uk (J. Li).

https://doi.org/10.1016/j.energy.2023.128963
Received 5 January 2023; Received in revised form 1 August 2023; Accepted 29 August 2023
Available online 31 August 2023

in the DVG application.

High-temperature ORC technology is attracting increasing attention for industrial waste heat recovery. Turboden, a company in the design and production of ORC systems, has been developing ORC solutions that run at up to 400 °C using the BDO mixture (such as Therminol® VP-1 and Dowtherm A) [16,17]. The systems allow an increase of about 15–20% of the net electrical performance as compared to those of the conventional ORCs, and achieve maximum efficiencies of 30–35% [16,17]. Superheat at the turbine inlet is not needed as the mixture is a dry fluid [18]. Despite the successful application in waste heat recovery, the potential of the BDO mixture as the power cycle fluid in the CSP application has not been explored yet.

The BDO mixture needs to overcome some foreseeable barriers before unlocking its potential. First, vapor generation under fluctuating solar radiation is challenging. The vapor generated at strong radiation is more than that at weak radiation. Without a reliable control strategy, the vapor temperature may exceed the permissible range. There is a high risk of temperature-related physical and chemical changes to the mixture in the collectors. Second, cost-effective storage is lacking. At present, long-term cost-effective storage is unavailable for commercial DSG systems [19,20]. If the water is replaced by the mixture in a conventional DSG system, it will face similar or even worse challenges as oil is more expensive than water. The sliding-pressure control strategy is commonly adopted for heat discharge of the direct systems. The temperature decrement attributed to flashing in the oil vessels during discharge will cause part-load operation of the entire thermodynamic cycle. The reason is that the decline of turbine intake temperature will cause an exponential decrease in the turbine intake pressure. The permitted temperature drop in a single tank will be limited (e.g., <50 °C) to avoid inefficient heat-to-power conversion [15], resulting in a limited and costly storage capacity. Third, the BDO mixture has low saturation pressure, which is only 4520 Pa at 150 °C and 4 Pa at 30 °C [21]. The vacuum is beyond practically achievable limits of 5000 Pa. A single-stage ORC using the mixture may not be more efficient than a conventional steam Rankine cycle (SRC).

A unique approach to thermal storage for DSG systems has been recently devised by the authors [15]. It allows a more significant water temperature drop. Upon completing a conventional first step discharge, the water in the high-temperature tank (HTT) is utilized to drive a bottom ORC. The thermodynamic cycles in the nominal and discharge processes are decoupled. The approach involves a particular second step discharge, which can enhance the storage capacity more than four times with an equivalent payback period of fewer than five years. As a result, long-term effective storage becomes possible for DSG plants. The decoupled thermodynamic cycles during charge and discharge processes also provide easy control of the solar field in fluctuating solar radiation conditions.

Table 1
Thermophysical properties of Therminol® VP-1 [5].

Property	Value, Units
Surface characteristic	Clear, water white liquid
Hightest permitted bulk temperature	400 °C
Hightest calculated film temperature	430 °C
Standard boiling point	257 °C
Solidification point	12 °C
Thermal expansivity @ 200 °C	0.000979/°C
Molecular weight (average)	166
Liquid density @ 15 °C/25 °C	1068 kg/m^3/1060 kg/m^3
Heat of vaporization @ 400 °C	206 kJ/kg
Kinematic viscosity @ 100 °C/40 °C	0.99 mm^2/s/2.48 mm^2/s
Critical temperature	499 °C
Critical pressure	33.1 bar

Inspired by the above method, this paper proposes an improved approach to tackle the challenges of the DVG systems by adopting two-stage oil tanks and cascade organic-steam Rankine cycle (ORC-SRC). The BDO mixture serves as the fluid for heat collection, thermal storage and power cycle. In the nominal condition, the mixture is vaporized directly in the collectors, and the saturated vapor from the top of HTT drives the ORC turbine. Meanwhile, the subcooled water from the bottom SRC is preheated and evaporated by the heat released from the ORC. The steam is further superheated and reheated by the liquid BDO mixture from the bottom of HTT before entering the steam turbines. In the discharge process, the liquid BDO mixture flows from the HTT to a low-temperature tank (LTT). The released sensible heat acts as the heat source for the bottom SRC.

To the authors' knowledge, it is the first time that thermal oil is

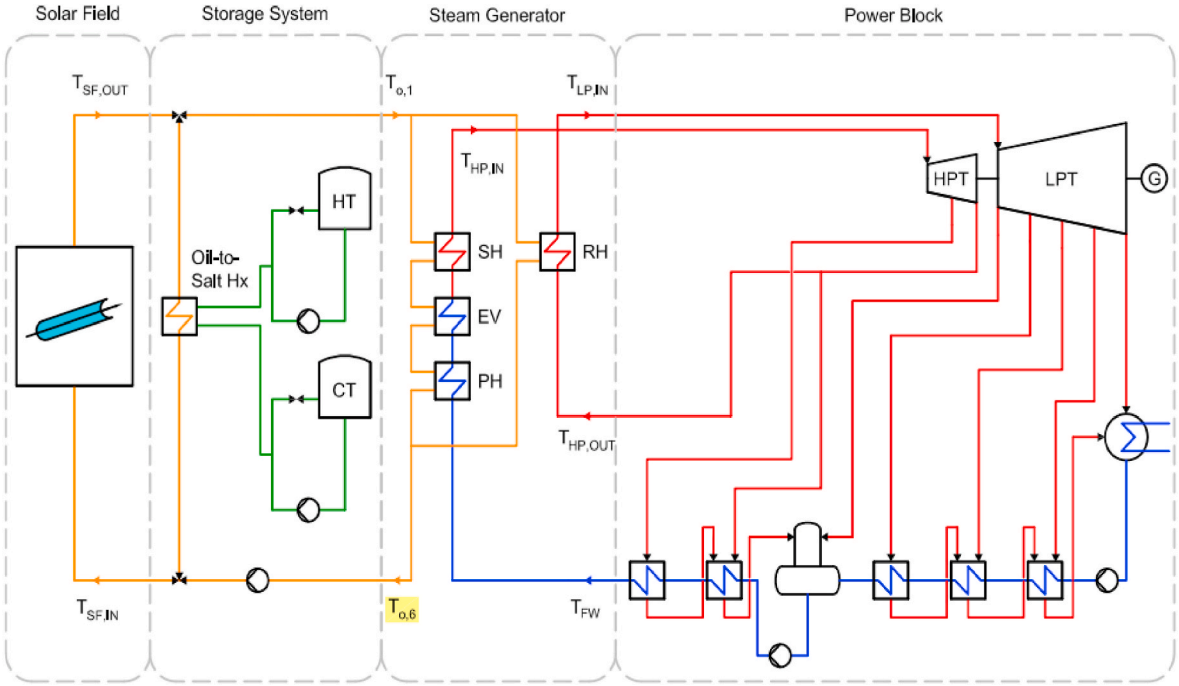

Fig. 1. Schematic plot of the PTC plant [3].

utilized as an ORC fluid in the CSP application. In the existing solar power plants, thermal oil is only adopted as the heat carrier and storage medium. Moreover, it is also the first time that thermal oil evaporates in the collectors for power conversion. The ORC is combined with a bottom SRC. Stable heat-to-power conversion can be guaranteed in the case of fluctuating solar irradiation, with a considerably extended storage capacity. Compared with the mainstream sole SRC-driven solar power systems, a higher thermal efficiency is achievable as the SRC is merely a part of the ORC-SRC. The oil-to-salt heat exchanger is omitted and the secondary heat transfer can thus be avoided. High heat collection and storage temperature can be facilitated owing to the much lower saturation pressure of the BDO mixture. For instance, the saturation pressure is only 0.959 MPa at 390 °C [21], while it is 5.5 MPa at 270 °C for water. The pressure-bearing difficulties existing in the steam vessels and vacuum tubes of traditional DSG systems are significantly alleviated. The cost of steel for the tanks will be smaller and the service life of the tubes will be extended. More details will be provided in the following sections.

The characteristics and operating principles of the novel system are illustrated in detail. Technical feasibility is elaborated, followed by the thermodynamic analysis in different operating modes. Finally, the equivalent payback time related to the additional investment on the ORC is analyzed.

2. System description

The schematic chart of the solar ORC-SRC is exhibited in Fig. 2. The system consists of the PTCs, HTT, LTT, and ORC-SRC unit. The BDO mixture in the HTT is in a state of vapor-liquid coexistence. The red box indicates the regular multistage extraction regenerative SRC. Two extractions, 11 and 12, are taken from the high-pressure (HP) turbine to the closed feedwaters (CF-1, CF-2). The closed feedwater heaters are shell-and-tube-type recuperators, which are utilized to elevate the feedwater temperature through condensation of the extracted steam. Four extractions, 15–18, are bled to a deaerator (open feedwater, OF) and three closed feedwaters (CF-3, CF-4, CF-5) from the low-pressure (LP) turbine. Deaerator is a direct contact-type heat exchanger in which streams at different temperatures are mixed to form a stream at an intermediate temperature [22]. Deaerators are also used for removing dissolved gases which can cause corrosion problems.

Fig. 3 presents the *T-s* curve of the cascade cycle. It can be seen that the BDO mixture behaves like a dry ORC fluid and it remains in superheated state during expansion. No complete saturated liquid curve or saturated vapor curve is displayed. The reason is that the thermophysical property data of the BDO mixture provided by the producer are in the range of up to 420 °C [21], which is far below its pseudocritical temperature of 499 °C.

The system can have several operating modes, determined by the HTT temperature (T_{HTT}) and the direct normal irradiance (I_{DN}). The follows are the two primary models.

Mode 1: Solar energy collection and cascade cycle operation are conducted simultaneously, as depicted in bold red in Fig. 4 (a). I_{DN} in the design condition is assumed to be 400 W/m^2, at which the total solar heat collection equals to the required rated heat of the ORC-SRC. The system runs in this situation when $I_{DN} \geq 400$ W/m^2. The subcooled BDO mixture from the LTT is heated in the PTCs and vaporized. The thermal oil at the collectors' outlet can be either in vapor, binary phase or liquid state depending on I_{DN}. But a saturated two-phase region state is more desirable to prevent the BDO mixture from overheating.

The ORC turbine is driven by the vapor gushing from the top of HTT. Meanwhile, the saturated steam is superheated and reheated by the liquid from the bottom of HTT before entering the two steam turbines. The residual solar energy can be stored in the HTT by increasing the oil's mass flow rate through P5 when irradiation intensity becomes strong. When $I_{DN} < 400$ W/m^2 (e.g., transient moment due to passing clouds), the system can still work in this mode. The T_{HTT} marginally drops from the rated value and flashing occurs inside the HTT for sliding pressure. The HTT acts as a Ruth's accumulator in this period and the ORC-SRC operates at off-design condition.

Mode 2: Heat discharge mode. The discharge process is similar to that of the two-tank indirect system in Fig. 1. As displayed in Fig. 4 (b), the BDO mixture flows from the HTT into the LTT and releases sensible heat to drive the bottom SRC.

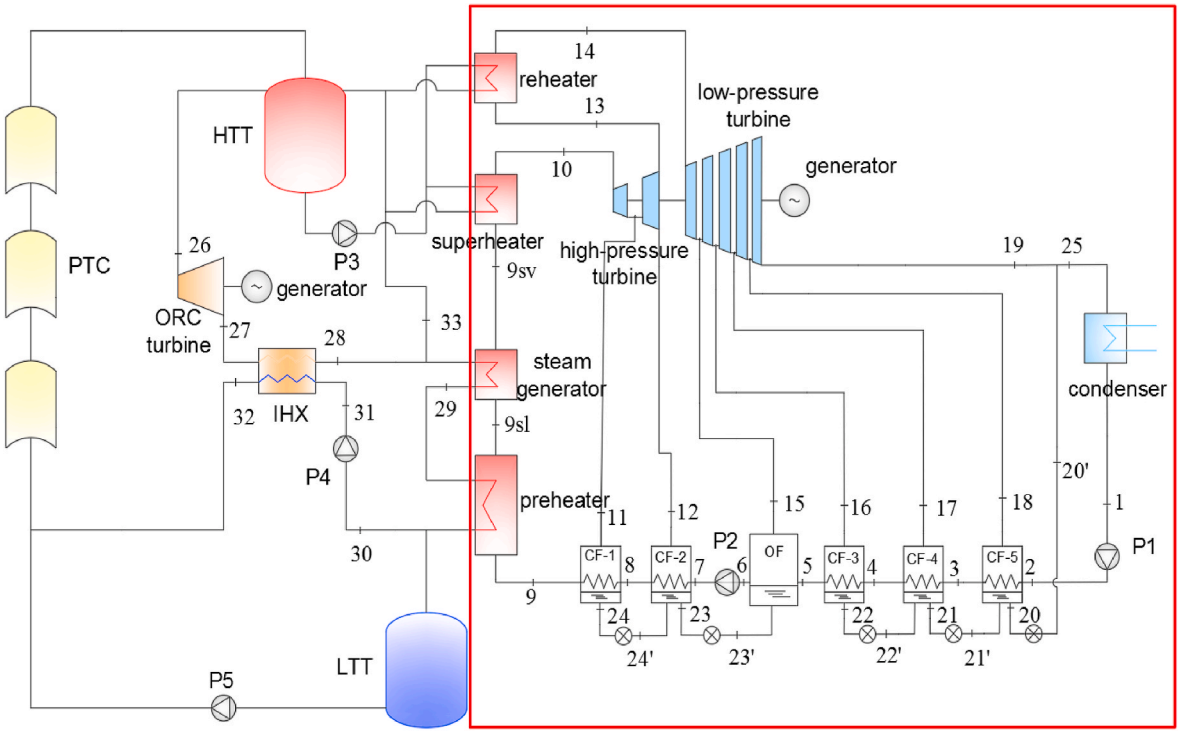

Fig. 2. Schematic chart of the solar ORC-SRC system.

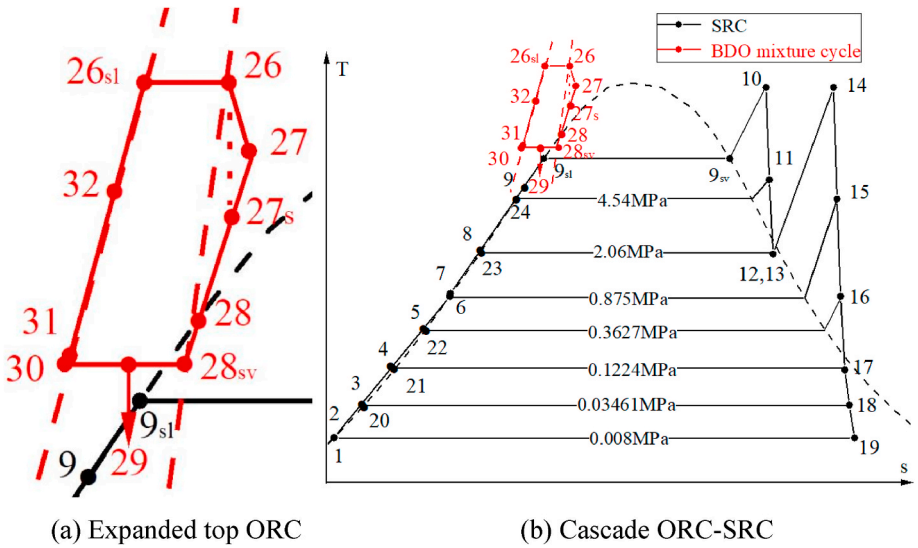

Fig. 3. *T-s* curve of the ORC-SRC.

The working condition (i.e., the state parameters and mass flow at each point) remains the same in the two modes for SRC. The total electricity generated by switching between the two modes is depicted in Fig. 5.

3. Technical feasibility

The BDO mixture is applicable in high-temperature ORC systems [5,16,17,23,24] and does not seem to have any technical barriers [25]. Experimental results also indicated the mixture had perfect stability after 5520–6000 h of repeated boiling/condensing cycles at nearly 380 °C [26,27]. But one challenge in solar ORC application is to prevent the formation of various contaminants (water, air, or degradation products). Water and oxygen/oxidizing agents can result in a faster increase in viscosity, and acids may accelerate the formation of volatile by-products. Oxidation by air shall be prevented. An expansion tank filled with nitrogen gas is generally in place to maintain the oil tanks positive pressure in conventional CSP plants, thereby preventing the air infiltration. It can also be applied to the proposed system. By filling nitrogen gas, the entire BDO mixture loops are sealed and free from contaminants. Another challenge is complicated control strategies associated with the need to generate superheated steam. Regarding the temperature control in the collectors, most solar radiation for PTCs is concentrated at the bottom section of the absorbers by the reflectors. The heat flux is higher at the bottom section, which is beneficial for the vaporization of the BDO mixture. The risk of the fluid temperature exceeding the permissible value is low. Particularly, the BDO mixture in the collectors is normally in a binary phase state and its wetness at the outlet is adjustable. No superheated vapor is generated. The saturated vapor is used to drive the ORC-SRC in the normal operation while the saturated liquid BDO mixture is stored in the HTT and later utilized to drive the bottom, conventional SRC when solar radiation is unavailable. The control of the solar field is flexible and straightforward.

4. Mathematical models

4.1. Thermodynamics

The thermodynamic states (1–33) are marked in Figs. 2 and 3. The equations for heat collection, heat transfer and power conversion are presented below.

4.1.1. Solar collectors

System Advisor Model software is employed to simulate the solar heat collection. The models for the optical efficiency, heat losses, irradiance incidence angle and overall efficiency of the PTCs are presented in Ref. [28].

4.1.2. Heat exchangers

The heat balance in the internal heat exchanger (IHX), preheater and steam generator is calculated by

$$h_{27} - h_{28} = h_{32} - h_{31} \tag{1}$$

$$m_{ORC}(h_{29} - h_{30}) = m_{steam}(h_{9sl} - h_9) \tag{2}$$

$$m_{ORC}(h_{28} - h_{29}) = m_{steam}(h_{9sv} - h_{9sl}) \tag{3}$$

where the subscripts *sv* and *sl* denote saturated vapor and saturated liquid, respectively.

For the preheater, the minimum temperature difference (ΔT_{min}) can only take place at the outlet of saturated water

$$T_{29} - T_{9sl} = T_{30} - T_{9sl} = T_{28sv} - T_{9sl} = \Delta T_{min} \tag{4}$$

The IHX efficiency (ε_{IHX}) is determined by

$$\varepsilon_{IHX} = \frac{h_{27} - h_{28}}{h_{27} - h(T_{31}, p_{28})} \tag{5}$$

where $h(T_{31}, p_{28})$ is the specific enthalpy of the BDO mixture at T_{31} (the pump's outlet temperature) and p_{28} (the condensation pressure). This would be the theoretical lowest enthalpy value to which the hot stream could be condensed. As $T_{30} = T_{28sv}$, $p_{28sv} = p_{28}$, and the liquid temperature increment after pressurization is limited, h (T_{31}, p_{28}) can be deemed as the saturated vapor enthalpy at T_{31}. The deduction of h_{27} and T_{28} will be given in Sections 5.1.6 and 5.4.2, respectively. Then T_{31} and h_{28} can therefore be obtained from Eqs. (8) and (9).

The terminal temperature difference, which is the difference between the saturation temperature of the extraction steam and the outlet temperature of feedwater, is assumed to be 1.5 °C [29].

$$T_{sv@p11} - T_9 = T_{sv@p12} - T_8 = T_{sv@p15} - T_6 = T_{sv@p16} - T_5 = T_{sv@p17} - T_4 = T_{sv@p18} - T_3 = 1.5 \tag{6}$$

The drain cooler approach, which is the difference between the outlet temperature of drain and the inlet temperature of feedwater, is assumed to be 5 °C [29].

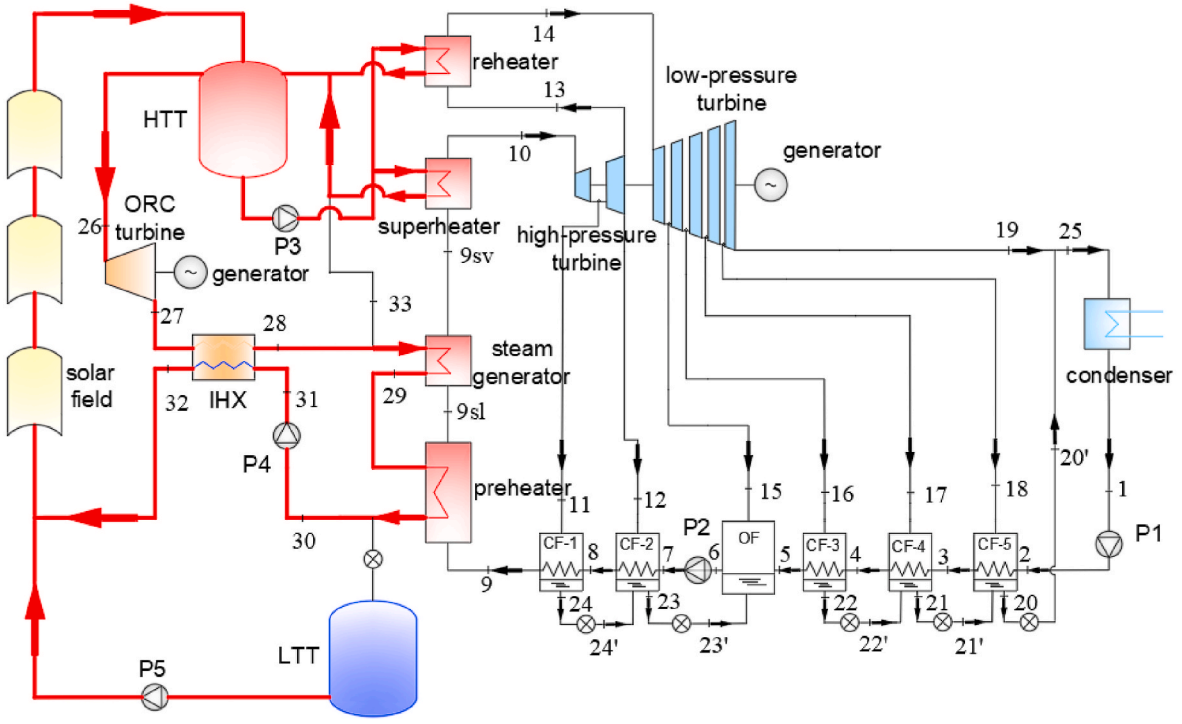

(a) Rated mode

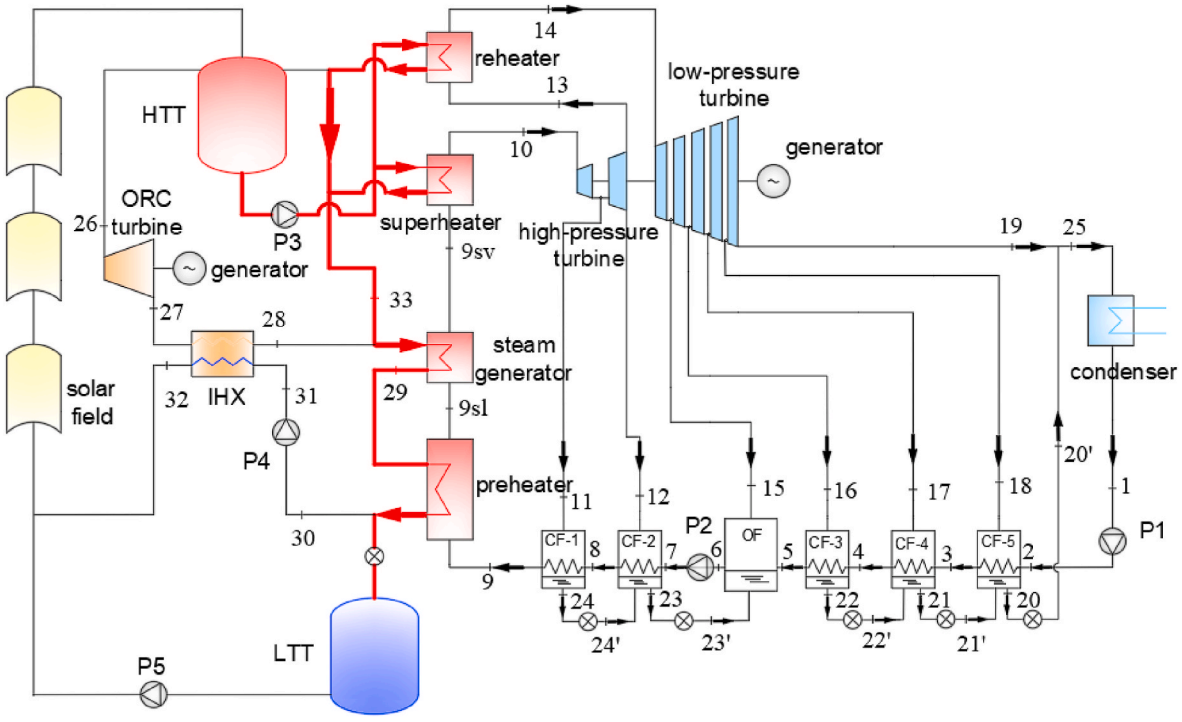

(b) Discharge mode

Fig. 4. Two different modes.

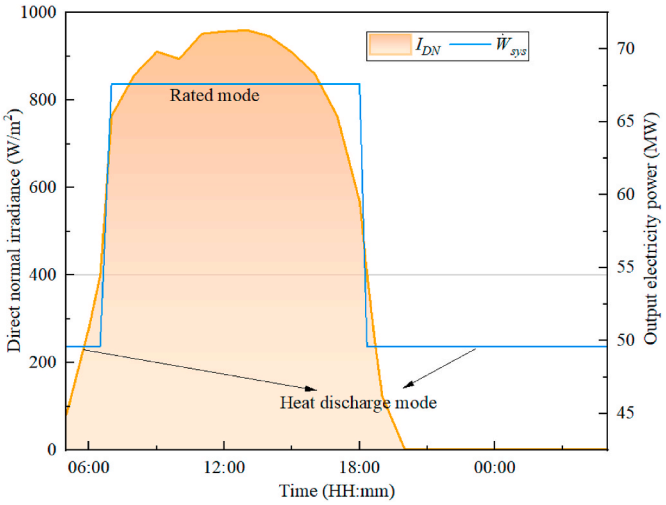

Fig. 5. Variations of I_{DN} and the two modes within 24 h.

$$T_{24}-T_8=T_{23}-T_7=T_{22}-T_4=T_{21}-T_3=T_{20}-T_2=5 \tag{7}$$

The energy conservation in CF-1 and CF-2 can be appraised by

$$m_{11}(h_{11}-h_{24})=m_{steam}(h_9-h_8) \tag{8}$$

$$m_{12}h_{12}+m_{24}h_{24'}+m_7h_7=m_8h_8+m_{23}h_{23} \tag{9}$$

The same is true for OF, CF-3, CF-4 and CF-5.

The condensed steam is throttled by throttle valves and flows into the neighboring feedwaters. The enthalpy of water after throttling is equal to that before throttling, $h_{24'}=h_{24}$, $h_{23'}=h_{23}$, $h_{22'}=h_{22}$ and $h_{21'}=h_{21}$.

The pressure drop in feed water extraction lines usually ranges from 2.5% to 3.5% [29]. In this study, the pressure drop is set at 3%.

4.1.3. Turbines

The mechanical work generated by the two steam turbines can be estimated as

$$W_{HT}=m_{steam}h_{10}-m_{11}h_{11}-m_{12}h_{12}-m_{13}h_{13} \tag{10}$$

$$W_{LT}=m_{14}h_{14}-m_{15}h_{15}-m_{16}h_{16}-m_{17}h_{17}-m_{18}h_{18}-m_{19}h_{19} \tag{11}$$

The specific enthalpy of each extraction can be obtained by the isentropic efficiencies of HP and LP turbines

$$\varepsilon_{HT}=\frac{h_{10}-h_{11}}{h_{10}-h_{11s}}=\frac{h_{11}-h_{12}}{h_{11}-h_{12s}} \tag{12}$$

$$\varepsilon_{LT}=\frac{h_{14}-h_{15}}{h_{14}-h_{15s}}=\frac{h_{15}-h_{16}}{h_{15}-h_{16s}}=\frac{h_{16}-h_{17}}{h_{16}-h_{17s}}=\frac{h_{17}-h_{18}}{h_{17}-h_{18s}}=\frac{h_{18}-h_{19}}{h_{18}-h_{19s}} \tag{13}$$

where s stands for isentropic.

The steam at the outlet of HP turbine is superheated, while the last stage of the LP turbine outlet is usually wet steam. ε_{LT} is related with steam wetness, as appraised by the Baumann rule, which is a long-standing empirical formula in the turbomachinery history [30,31].

$$\varepsilon_{LT}=\varepsilon_{LT,sh}(1-ay_{av}) \tag{14}$$

$$y_{av}=(y_{14}+y_{19})/2 \tag{15}$$

where $\varepsilon_{LT,sh}$ is the reference isentropic efficiency supposing that the inlet and outlet of LP turbine are superheated steam; a is the Baumann factor and its common value is 1.0 [31]; y_{14} and y_{19} are respectively the wetness of live and exhaust steam.

For the HP turbine, a higher inlet pressure leads to greater steam density, smaller volume flow rate, less nozzle flow passage area and lower specific speed. The corresponding nozzle and moving blade losses, blade height loss, leakage loss, impeller friction loss and other losses have negative effects on the efficiency, and finally results in a lower turbine isentropic efficiency.

For the ORC turbine,

$$W_{OT}=m_{ORC}(h_{26}-h_{27})=m_{ORC}(h_{26}-h_{27s})\varepsilon_{OT} \tag{16}$$

where ε_{OT} denotes the isentropic efficiency of ORC turbine.

4.1.4. Pumps

The consumed work by P1, P2 and P4 is obtained by

$$W_{P1}=m_1(h_2-h_1)=m_1(h_{2s}-h_1)/\varepsilon_P \tag{17}$$

$$W_{P2}=m_{steam}(h_7-h_6)=m_{steam}(h_{7s}-h_6)/\varepsilon_P \tag{18}$$

$$W_{P4}=m_{ORC}(h_{31}-h_{30})=m_{ORC}(h_{31s}-h_{30})/\varepsilon_P \tag{19}$$

where ε_P is the pump efficiency.

4.1.5. Entropy of BDO mixture in saturated state

The high-quality BDO mixture brands include Therminol® VP-1 (US), Dowtherm-A (US), Therm-S-300 (Japan) and Diphyl (Germany). The datasheet of Therminol® VP-1 supplied by Eastman Corp is employed in this paper for the thermophysical properties. The saturated liquid and vapor parameters at intervals of 10 °C can be acquired [21]. Eastman Corp has a strong foundation of more than semicentury in industry production, and it provides high-quality fluids backed by expert technical support which are adopted by more than 15,000 projects around the world [32]. The saturation state parameters (like T, p, h, v) at different temperatures can be calculated by linear interpolation.

The manufacturer's datasheet provides the enthalpy in saturated liquid and vapor states, together with temperature, pressure, and specific volume. The entropy is not directly provided. However, it can be derived from thermodynamic relation.

$$dh=Tds+vdp \tag{20}$$

As entropy or specific entropy is a state parameter, the selection of the reference state will have no impact on the thermodynamic calculation results of ORC. The turbines' efficiencies are related to the change of entropy rather than the absolute value. It is assumed that the saturation entropy of BDO mixture at 313.34 °C is $s_{30}=s_{313.34°C,sl}=3$ kJ/kg·K. The reference temperature of 313.34 °C is chosen because it can be a cold side temperature of the ORC, which is 10 °C above the steam evaporation temperature in a common CSP system using thermal oil.

4.1.6. Enthalpies of BDO mixture at the outlets of ORC turbine and IHX

The enthalpy of BDO mixture in superheated state is not provided in the manufacturer's datasheet. The information is generally necessary in modelling the ORC efficiency. As shown in Eq. (16), the enthalpy at point 27 is required to calculate the output work of turbine, which is beyond the saturation vapor curve. It is difficult to apply a conventional ORC efficiency model without the parameters in superheated state. To overcome this problem, the authors have put forward an ORC efficiency model based on the equivalent hot side temperature (T_{EHST}) [33], in which only the saturated parameters are required.

$$T_{EHST}\approx\frac{h_{26}-h_{30}-v_{30}(p_{26}-p_{30})}{s_{26}-s_{30}} \tag{21}$$

The ORC efficiency in a basic structure ($\eta_{ORC,b}$) can be built with the assistance of T_{EHST}. $\eta_{ORC,b}$ shows a good match with the actual value. The relative error ranges from −0.7% to 3.4% for 27 fluids [33].

$$\eta_{ORC,b}=\left(1-\frac{T_{30}}{T_{EHST}}\right)\cdot\frac{\varepsilon_{OT}\cdot\varepsilon_g+v_{30}(p_{26}-p_{30})\Big/\left(\varepsilon_P\cdot\int_{26}^{28sv}v_{sv}dp\right)}{1+v_{30}(p_{26}-p_{30})\Big/\left(\int_{26}^{28sv}v_{sv}dp\right)} \tag{22}$$

where $\int_{26}^{28sv} v_{sv}dp$ can be calculated by piecewise integration and then summation.

$$\int_{26}^{28sv} v_{sv}dp = \int_{390}^{380} v_{sv}dp + \int_{380}^{370} v_{sv}dp + \cdots + \int_{330}^{320} v_{sv}dp + \int_{320}^{313.34} v_{sv}dp \tag{23}$$

Meanwhile, $\eta_{ORC,b}$ can be expressed as

$$\eta_{ORC,b} = \frac{(h_{26} - h_{27})\cdot\varepsilon_g - (h_{31} - h_{30})}{h_{26} - h_{31}} \tag{24}$$

The majority of ORC fluids are not compressible in liquid state, and the condensation process can carry away most of the heat [33]. In consequence,

$$h_{31s} \approx h_{30} + v_{30}(p_{31s} - p_{30}) \tag{25}$$

where $p_{31s} = p_{31} = p_{32} = p_{26} =$ 0.959 MPa. p_{30}, h_{30} and v_{30} can be deduced by linear interpolation. h_{27} can be derived by calculating Eqs. (19) and (21-25) as the ideal electricity generated is associated with ORC efficiency and the heat input.

With the heat recovered from the IHX (m_{ORC} ($h_{32} - h_{31}$)) and the electricity generation of a basic ORC, the ORC efficiency with the IHX can be estimated below.

4.1.7. Thermal efficiency

The bottom SRC represents the traditional dual-tank structure system. Its thermal efficiency can be defined as

$$\eta_{SRC} = \frac{W_{SRC}}{Q_{SRC}} = \frac{(W_{HT} + W_{LT})\cdot\varepsilon_g - W_{P1} - W_{P2}}{m_{steam}(h_{10} - h_9) + m_{13}(h_{14} - h_{13})} \tag{26}$$

The heat-to-power conversion efficiency of the top ORC can be determined by

$$\eta_{ORC} = \frac{W_{ORC}}{m_{ORC}(h_{26} - h_{32})} = \frac{W_{OT}\cdot\varepsilon_g - W_{P4}}{m_{ORC}(h_{26} - h_{32})} \tag{27}$$

The thermal efficiency of the cascade ORC-SRC is defined by

$$\eta_{ORC-SRC} = \frac{W_{ORC-SRC}}{Q_{ORC-SRC}} = \frac{W_{ORC} + W_{SRC}}{m_{steam}(h_{10} - h_{9sv}) + m_{13}(h_{14} - h_{13}) + m_{ORC}(h_{26} - h_{32})} \tag{28}$$

4.1.8. Operating duration of the bottom SRC

Given the mass of BDO mixture in the storage tank, the duration of the bottom SRC operation during the heat discharge mode can be described by

$$t_{SRC} = \frac{M_{BDO}}{m_d} \tag{29}$$

where t_{SRC} represents storage capacity; M_{BDO} is the mass of BDO mixture in the HTT; and m_d is the discharge flow rate, which can be derived from the heat balance in the steam generator, reheater and superheater.

$$m_d = \frac{m_{steam}(h_{10} - h_{9sl}) + m_{13}(h_{14} - h_{13})}{h_{26sl} - h_{29,d}} \tag{30}$$

where $h_{29,d}$ stands for the enthalpy of point 29 during discharge. It is worth noting that $h_{29,d}$ differs from h_{29} because point 29 is in liquid state during discharge, and it is in binary-phase state under the rated mode. T_{29} can be acquired from Eq. (4) and then $h_{29,d}$ is obtained by linear interpolation.

The electricity generated by 1 kg BDO mixture from the HTT to the LTT in the discharge mode is calculated by

$$w_{BDO} = \frac{(h_{HTT} - h_{LTT})\eta_{SRC}}{3600} \tag{31}$$

4.1.9. Equivalent heat-to-power efficiency

In order to comprehensively consider the efficiencies in the nominal and discharge conditions, an equivalent heat-to-power efficiency is introduced [34,35], and is expressed by

$$\eta_{eq} = \frac{W_{total}}{Q_{total}} = \frac{t_{ORC-SRC}(W_{ORC} + W_{SRC}) + t_{SRC}W_{SRC}}{t_{ORC-SRC}Q_{ORC-SRC} + t_{SRC}Q_{SRC}} \tag{32}$$

where $t_{ORC-SRC}$ is the ORC-SRC operating time. η_{eq} comprehensively reflects the performance of ORC-SRC system. From the perspective of thermodynamics, it implies how effectively the collected solar heat, including that stored in HTT, is converted into power output [34,35].

4.2. Thermo-economics

It is difficult to accurately assess the overall investment and payback period of the novel system on account of its complexity. Alternately, a conventional SRC system based on dual-tank thermal oil structure (such as SEGSIor SEGSII) is taken as a reference. The economic superiorities of the novel system in Fig. 2 will be outlined through a comparison with the reference. The proposed system can facilitate generation of excess electricity each year at the cost of extra ORC investment. Thus an equivalent payback period (*EPP*) with respect to the additional ORC is defined as

$$EPP = \frac{C_{add}}{Y} \tag{33}$$

where C_{add} is the added cost due to installing the ORC, and Y is the excess annual yield. C_{add} includes the investments in supplementary PTCs, IHX, ORC turbine, ORC generator and P4.

For a better comparison, it is assumed that the operation conditions including temperature, pressure, flow rate and power output of the bottom SRC in the proposed system are the same as those in the reference system. Since common dual-tank systems are equipped with 7.5 h of storage [3], given the same discharge duration of 7.5 h, the electricity generated by the two systems during the discharge process are the same. Therefore, Y is only attributed to the difference of output under the rated mode. Determining the *EPP* is reasonable by

$$EPP = \frac{C_{PTC} + C_{IHX} + C_{OT} + C_{ORC,g} + C_{P4}}{Y_{rated,ORC-SRC} - Y_{rated,ref}} \tag{34}$$

Each term in Eq. (34) is clarified below.

4.2.1. Cost of supplementary PTCs (C_{PTC})

The total aperture area of a CSP system consists of the area required by both rated and discharge modes. The latter is the same for the two systems due to the same discharge working condition and duration. The extra cost for the former is

$$C_{PTC} = P_{PTC}\cdot\left(A_{PTC,ORC-SRC} - A_{PTC,ref}\right) \tag{35}$$

where P_{PTC} is the PTC price per square meter, and A_{PTC} is the required PTC area in the nominal condition.

Assume that the runtime of both systems under the rated condition is 8 h, i.e., $t_{ORC-SRC} = t_{ref} = 8$ h. A_{PTC} is respectively expressed by

$$A_{PTC,ORC-SRC} = \frac{Q_{ORC-SRC}\cdot t_{ORC-SRC}}{t_{s,st}\cdot I_{DN,st}\cdot\eta_{PTC,st,ORC-SRC}} \tag{36}$$

$$A_{PTC,ref} = \frac{Q_{SRC}\cdot t_{ref}}{t_{s,st}\cdot I_{DN,st}\cdot\eta_{PTC,st,ref}} \tag{37}$$

where $t_{s,st}$ is the standard sunshine duration (h); $I_{DN,st}$ is the standard direct normal solar irradiance (kW/m^2) and $\eta_{PTC,st}$ is the standard PTC efficiency.

4.2.2. Cost of IHX (C_{IHX})

The precise calculation steps of the IHX area and the corresponding cost are presented in the authors' previous work [28]. The actual cost needs to be converted from the cost of 2001 by calculating the Chemical Engineering Plant Cost Index (*CEPCI*) [36]. The cost of 2018 should be corrected as

$$C_{BM,2018} = C_{BM,2001} \cdot CEPCI_{2018} / CEPCI_{2001} \tag{38}$$

where $CEPCI_{2001} = 397$, $CEPCI_{2018} = 648.7$.

4.2.3. Cost of ORC turbine (C_{OT}), P4 (C_{P4}) and ORC generator ($C_{ORC,g}$)

The purchased cost of turbine and pump is [37].

$$log_{10} C_P = K_1 + K_2\, log_{10}\, W + K_3 (log_{10}\, W)^2 \tag{39}$$

where C_p is a basic cost concerning with the work output or consumption. K_1, K_2, and K_3 are coefficients and their values are displayed in Ref. [28]. The bare module cost of pump is calculated by Eq. (30) in Ref. [28]. The bare module cost of ORC turbine is [37]

$$C_{BM,OT} = C_P F_{BM} F_P \tag{40}$$

The cost of ORC generator is [38].

$$C_{ORC,g} = 60\left(\varepsilon_g W_{OT}\right)^{0.95} \tag{41}$$

4.2.4. Annual revenues in the rated mode for ORC-SRC ($Y_{rated,ORC-SRC}$) and the reference system ($Y_{rated,ref}$)

The annual yield is

$$Y_{rated,ORC-SRC} = P_e \cdot \eta_{ORC-SRC} \cdot \sum_{1}^{8760} \left(\eta_{PTC,ORC-SRC} \cdot I_{DN} \cdot A_{PTC,ORC-SRC}\right) \tag{42}$$

$$Y_{rated,ref} = P_e \cdot \eta_{SRC} \cdot \sum_{1}^{8760} \left(\eta_{PTC,SRC} \cdot I_{DN} \cdot A_{PTC,ref}\right) \tag{43}$$

where P_e is the electricity price.

5. Results and discussion

Only subcritical Rankine cycles are considered, because a constant pressure and temperature in the evaporation process can be maintained.

Table 2
Fixed parameters in calculation.

Term	Value
Gross electric power of SRC [22], $(W_{HT} + W_{LT}) \cdot \varepsilon_g$	50 MW
HP turbine efficiency [22,39], ε_{HT}	0.855
LP turbine efficiency [22,39], ε_{LT}	0.895
Pressure of extraction no. 1 [39], p_{11}	4.54 MPa
Pressure of extraction no. 2 [39], p_{12}	2.06 MPa
Pressure of extraction no. 3 [39], p_{15}	0.875 MPa
Pressure of extraction no. 4 [39], p_{16}	0.3627 MPa
Pressure of extraction no. 5 [39], p_{17}	0.1224 MPa
Pressure of extraction no. 6 [39], p_{18}	0.03461 MPa
Steam condensation pressure [22,39], p_{19}	0.008 MPa
Pressure drop in feed water extractions lines [28]	3%
HP turbine inlet temperature [39], T_{10}	370 °C
HTT temperature [40], T_{HTT}	390 °C
Minimum heat transfer temperature difference [40], ΔT_{min}	10 °C
ORC turbine efficiency [40], ε_{OT}	0.85
Generator efficiency [15], ε_g	0.95
Pump efficiency [41], ε_P	0.75
Internal heat exchanger efficiency [41], ε_{IHX}	0.8
Runtime of ORC-SRC [31], $t_{ORC-SRC}$	8 h
Standard direct normal solar irradiation [15], $I_{DN,st}$	0.8 kW/m^2
Standard wind speed [15], $v_{w,st}$	5 m/s
Standard ambient temperature [41], T_a	25 °C
Price of PTC [42], P_{PTC}	170 $/m^2
Price of electricity [15], P_e	0.184 $/kWh

Some hypotheses are made as listed in Table 2.

The SRC evaporation temperature (T_{9sv}) is a vital parameter because it affects not only the cascade cycle efficiency ($\eta_{ORC-SRC}$) in the nominal operation condition, but also the bottom cycle efficiency (η_{SRC}) in the discharge process. In this simulation, T_{9sv} varies from 260 °C to 310 °C based on the following considerations. First, a higher live steam temperature and pressure correspond to a higher power cycle efficiency, but result in greater technological challenges and higher investment cost of the steam turbine. The power blocks of state-of-the-art PTC plants adopting conduction oils have live steam temperature and pressure of 380 °C/10 MPa (the corresponding steam evaporation temperature is 311 °C) and the available turbine manufacturers include Man-Turbo and Siemens [3]. The upper limit of T_{9sv} is selected as 310 °C. Second, the minimum inlet steam pressure (p_{10}) is theoretically higher than the first stage suction pressure (p_{11}) of 4.54 MPa (the corresponding saturation temperature is 257.98 °C). The lower limit of T_{9sv} is chosen as 260 °C. The simulation below will also show that T_{9sv} corresponding to the maximum $\eta_{ORC-SRC}$ is not lower than 260 °C.

5.1. Thermodynamic performance of ORC-SRC in the rated mode

All the flow rates correlated with the turbines are illustrated in Figs. 6 and 7. The flow rates of main steam (m_{10} or m_{steam}), reheating (m_{13}) and condensing (m_{19}) go down almost linearly while the ORC flow rate (m_{ORC}) first drops and then climbs. With the increment in T_{9sv}, the electricity output of the SRC turbines per kilogram of steam rises. m_{10} falls down as the gross electric power of SRC is fixed at 50 MW. The flow rates of each extraction are much lower than m_{10}, m_{13} or m_{19}, and range from about 2.0 to 6.0 kg/s. As $m_{13} = m_{10} - m_{11} - m_{12}$, the decline of m_{10} is greater than the sum of m_{11} and m_{12}, and thereby m_{13} goes down as depicted in Fig. 6. The same is true for m_{19}. The variation of m_{ORC} is because the total heat input from ORC to SRC $m_{steam}(h_{9sv} - h_9)$ drops

Table 3
Thermodynamic parameters of each state point when $T_{9sv} = 260$ °C.

State point	Temperature (°C)	Pressure (MPa)	Enthalpy (kJ/kg)	Quality (%)
1	41.51	0.008	173.84	0
2	41.60	0.875	175	subcooled
3	70.92	0.875	297.60	subcooled
4	103.86	0.875	436.02	subcooled
5	138.61	0.875	583.55	subcooled
6	172.66	0.875	730.76	subcooled
7	173.49	4.692	736.43	subcooled
8	212.38	4.692	909.40	subcooled
9	256.48	4.692	1117.50	subcooled
10	370	4.692	3128.10	superheated
11	365.44	4.54	3119.86	superheated
12	265.43	2.06	2939.63	superheated
13	265.43	2.06	2939.63	superheated
14	370	2.06	3181	superheated
15	265.37	0.875	2980.97	superheated
16	174.32	0.3627	2808.80	superheated
17	105.36	0.1224	2633.38	97.75
18	72.42	0.03461	2457.08	92.56
19	41.51	0.008	2279.26	87.64
20	46.60	0.03357	195.16	subcooled
21	75.92	0.11873	317.94	subcooled
22	108.86	0.35182	456.75	subcooled
23	178.46	1.9982	756.92	subcooled
24	217.38	4.4038	932.13	subcooled
25	41.51	0.008	1932.26	73.20
26_{sl}	390	0.959	774.40	0
26	390	0.959	987.60	100
27	344.43	0.133	928.62	superheated
28	288.04	0.133	806.14	superheated
28_{sv}	270	0.133	773.80	100
29	270	0.133	489.63	–
30	270	0.133	486.30	0
31	271	0.959	487.60	subcooled
32	322.59	0.959	610.08	subcooled

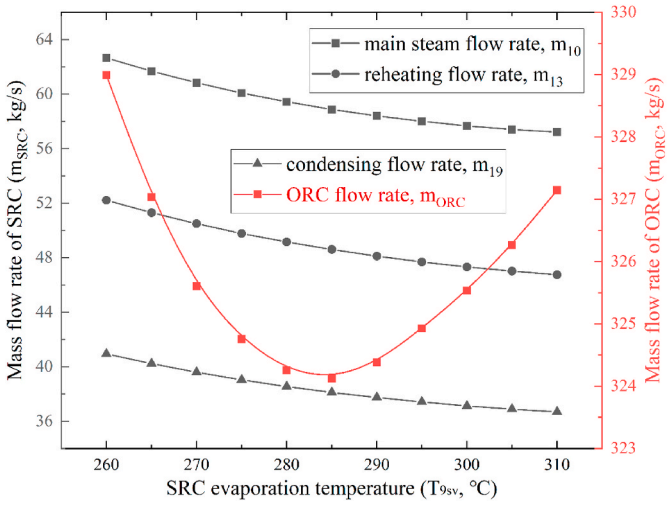

Fig. 6. Variations of the flow rates of main steam, reheating, condensing and ORC.

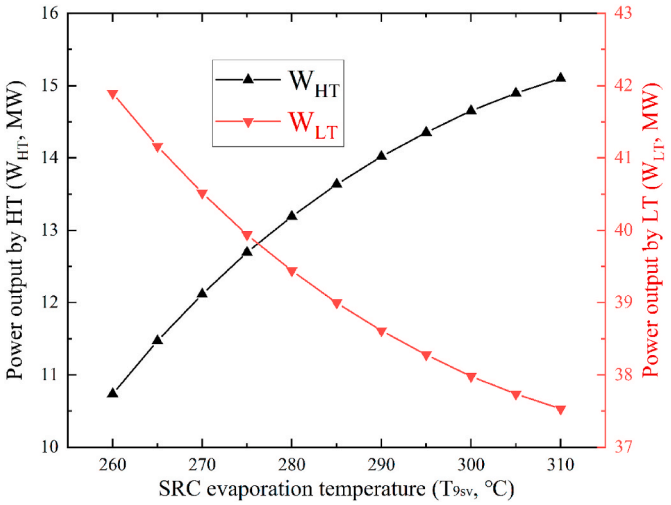

Fig. 8. Variations of the power output by the two steam turbines.

significantly while the latent heat of BDO mixture for condensation ($h_{28sv} - h_{30}$) varies slightly. For example, $m_{steam}(h_{9sv} - h_9)$ is 105.22, 97.53 and 92.16 MW respectively at T_{9sv} of 260, 285 and 310 °C, while ($h_{28sv} - h_{30}$) is respectively 287.5, 274.0 and 259.7 kJ/kg.

The relative decrements of the extracted steam in the LP turbine are about 10%, which are similar to those of m_{19}. According to the heat balance in OF, CF-3, CF-4 and CF-5, a decreased m_{19} results in a smaller extraction rate. However, the flow rates of the extracted steam in the HP turbine are flatter, especially for m_{11}. The change in m_{11} is caused by another conflicting factor working in conjunction with m_{19}. In this simulation the extraction pressures are fixed despite a variable steam pressure at the HP turbine inlet. A higher T_{9sv} is accompanied by a higher live steam pressure (p_{10}) while a constant temperature of 370 °C. Given the extraction pressure, T_{11} decreases with a larger steam pressure ratio during expansion in the HP turbine. h_{11} consequently drops, which tends to cause a higher m_{11}.

Variations of the electricity output by the two steam turbines are graphed in Fig. 8. W_{HT} increases while W_{LT} decreases as T_{9sv} climbs. W_{LT} is approximately 2.5–4.0 times as much as W_{HT}. The reason for the increment in W_{HT} can be obtained by the variations of mass flow rates and enthalpy values. Both m_{10} and m_{13} decrease and the difference between them is approximately constant as T_{9sv} increases, and the changes in m_{11} and m_{12} are slight. Meanwhile, h_{10}, h_{11}, h_{12} and h_{13} ($h_{12} = h_{13}$) decline as T_{9sv} elevates. But the magnitude of the decline in h_{11}, h_{12} and h_{13} is larger than that in h_{10}. For instance, the difference between h_{10} and h_{12} is 188.47, 215.68, 237.80 kJ/kg when T_{9sv} is 260, 270, 280 °C, respectively. Although m_{10} declines, W_{HT} rises with T_{9sv} because of a larger enthalpy drop of the HP turbine. The decrement in the W_{LT} is attributed to the decreasing m_{13} and the increasing W_{HT}.

Variations of the net electricity output of ORC and SRC are exhibited in Fig. 9. W_{SRC} declines marginally while W_{ORC} reduces considerably as T_{9sv} elevates. Given total electricity output of the steam turbines of 50 MW, the increment in T_{9sv} leads to more water pump power consumption, so W_{SRC} is slightly reduced. The ORC condensation temperature climbs and η_{ORC} drops as T_{9sv} rises, and thus W_{ORC} reduces. W_{SRC} is approximately 2.56–5.21 times as high as W_{ORC}. W_{SRC} is 49.59 MW and W_{ORC} is 19.41 MW at the optimal condition of $T_{9sv} = 260$ °C.

The higher efficiency results from a higher average heat absorbing temperature of the cascade cycle. The heating process of the ORC-SRC is composed of three parts: 1) the BDO mixture enthalpy increment from state point 32 to point 26; 2) the steam enthalpy increment from point 9sv to point 10; and 3) the steam enthalpy increment from point 13 to point 14. For a conventional SRC, the heating process consists of two

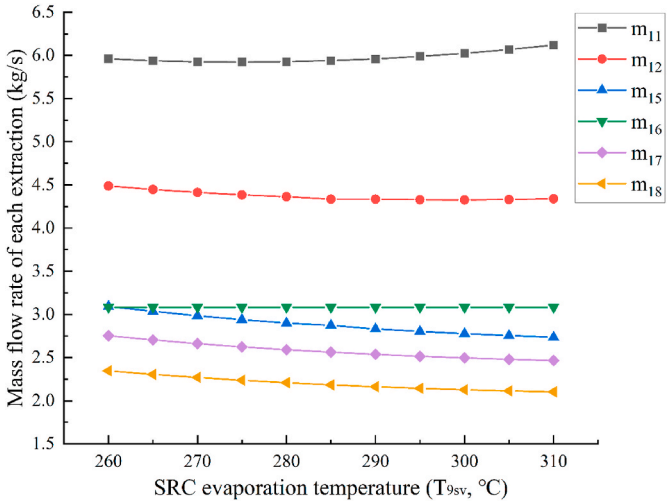

Fig. 7. Variations of the flow rate of each extraction.

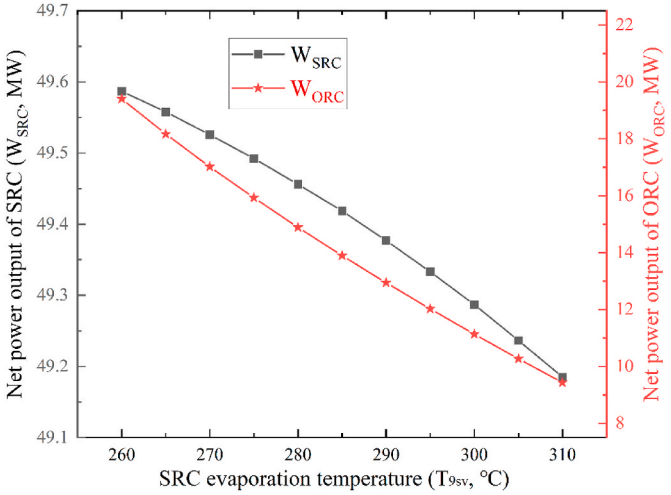

Fig. 9. Variations of the net power output of ORC and SRC.

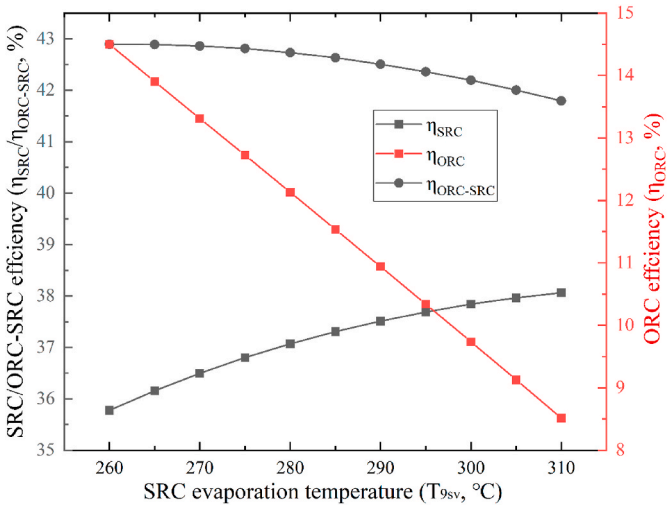

Fig. 10. Variations of SRC, ORC and ORC-SRC efficiencies η_{ORC}, η_{SRC} and $\eta_{ORC-SRC}$ are presented in Fig. 10. Given T_{HTT} and steam condensation pressure (p_{19}), both T_{EHST} for the SRC and the equivalent cold side temperature for the ORC increase as T_{9sv} rises, resulting in increasing η_{SRC} and declining η_{ORC}. $\eta_{ORC-SRC}$ is a compromise between η_{ORC} and η_{SRC}. The maximum $\eta_{ORC-SRC}$ of 42.90% is achieved at T_{9sv} of 260 °C. The relevant parameters under this optimal rated mode are summarized in Table 3. Notably, a T_{9sv} of 260 °C will be beneficial for the steam turbines because the tip-leakage flow loss in the HP turbine can be reduced as compared to a traditional one operating at 10 MPa. Given T_{10}, the steam wetness during expansion also reduces and a higher turbine efficiency is expected.

parts: 1) the water/steam enthalpy increment from point 9 to point 10; and 2) the steam enthalpy increment from point 13 to point 14. The average absorbing temperatures of the two cycles can be expressed by:

$$T_{av,ORC-SRC} = \left(m_{ORC} \int_{32}^{26} Tds + m_{10} \int_{9sv}^{10} Tds + m_{13} \int_{13}^{14} Tds \right) \Big/ \left[m_{ORC}(s_{26} - s_{32}) + m_{10}(s_{10} - s_{9sv}) + m_{13}(s_{14} - s_{13}) \right] \quad (44)$$

$$T_{av,SRC} = \left(\int_{9}^{10} Tds + \int_{13}^{14} Tds \right) \Big/ (s_{10} - s_9 + s_{14} - s_{13}) \quad (45)$$

Based on the above expression, $T_{av,ORC-SRC}$ at T_{9sv} = 260 °C is 363 °C, while $T_{av,SRC}$ is 273 °C for a conventional SRC.

5.2. Thermodynamic performance of ORC-SRC in the discharge mode

The proposed system has a similar discharge process to a conventional CSP system. A difference is that a lower water evaporation temperature is achieved. Variations of the LTT temperature (T_{LTT}), discharge flow rate (m_d) and power output by per kg mass of BDO mixture (w_{BDO}) are depicted in Fig. 11. m_d increases as T_{9sv} climbs owing to the temperature increment in BDO mixture leaving the steam generator and preheater. The temperature gap between the two tanks decreases. The discharge capacity (t_{SRC}) is inversely proportional to m_d according to Eq. (29). It indicates that a lower T_{9sv} leads to a longer discharge duration at a given storage mass (M_{BDO}). For example, given M_{BDO} of 2000 tonnes, t_{SRC} declines from 1.164 h to 0.851 h when T_{9sv} rises from 260 °C to 310 °C. Similarly, t_{SRC} reduces from 10.476 h to 7.661 h when M_{BDO} is 18,000 tonnes.

In typical PTC plants, the storage temperature varies from 293 °C to 393 °C [20], and the steam evaporation temperature is approximately 310 °C to achieve efficient power conversion in the normal operating conditions. The storage capacity is not maximized. Most heat is transferred to the binary phase region on account of the huge latent heat of water. In order to avoid an uneconomically low efficiency, the LTT temperature is relatively high (293 °C). In contrast, the ORC-SRC can simultaneously provide lower T_{LTT} and T_{9sv}. The power generation per kg of storage fluid increases as T_{9sv} decreases, as shown in Fig. 11. The relative storage capacity in MWe is increased by about 38% when T_{9sv} goes down from 310 °C to 260 °C. A significant temperature drop of more than 100 °C from HTT to LTT is available when T_{9sv} is lower than 288 °C. A lower T_{9sv} results in a decreased η_{SRC}, but a significantly larger

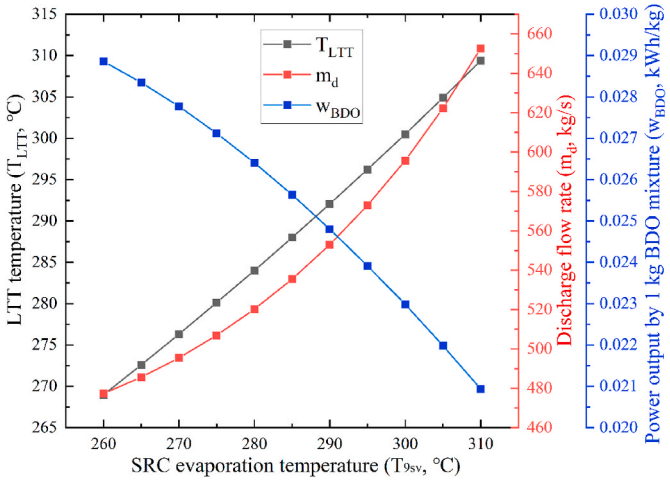

Fig. 11. Variations of T_{LTT}, m_d and w_{BDO} in the heat discharge process.

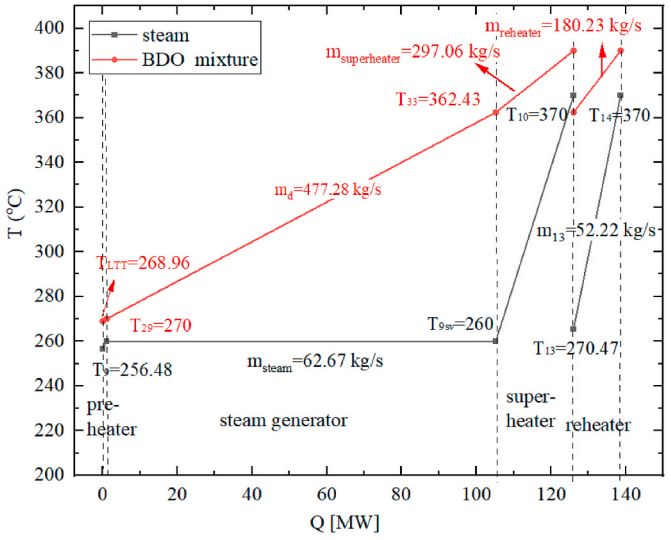

Fig. 12. *T-Q* chart during the discharge process at T_{9sv} of 260 °C.

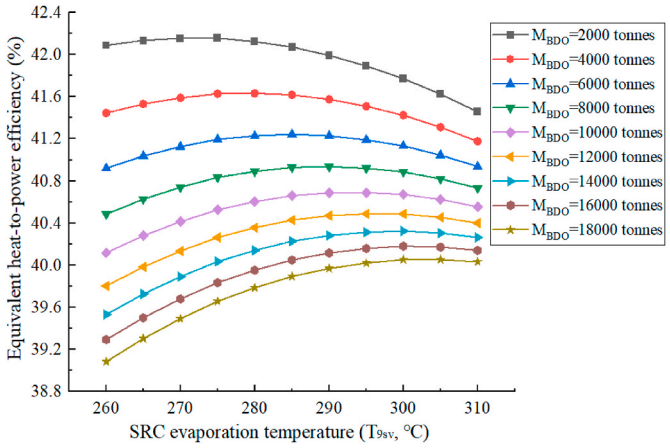

Fig. 13. Variations of η_{eq} at different mass of storage BDO mixture.

storage capacity and a greater temperature difference between the two tanks. It will also offer a higher $\eta_{ORC-SRC}$. From this viewpoint, a lower T_{9sv} seems to be more beneficial to the ORC-SRC.

Assume the BDO mixture temperatures at the outlets of both reheater and superheater are the same (equal to T_{33}), the *T-Q* diagram when $T_{9sv} = 260$ °C is graphed in Fig. 12. The four heat exchangers are divided by five dotted lines. T_{LTT} is 268.96 °C, which is approximately 24 °C lower than that of a conventional LTT.

5.3. Equivalent heat-to-power efficiency

The power conversion in both charge and discharge processes can be comprehensively reflected by the equivalent heat-to-power efficiency (η_{eq}), and it can represent the overall efficiency of the system. η_{eq} is influenced by both T_{9sv} and the total storage mass (M_{BDO}). Its variation is graphed in Fig. 13. As the efficiency during discharge (η_{SRC}) is lower than that in the normal operation ($\eta_{ORC-SRC}$), a shorter t_{SRC} and less M_{BDO} leads to a higher η_{eq}. But the amount of electricity generated during discharge is also reduced. The peak η_{eq} drops from 42.16% to 40.03% and the corresponding T_{9sv} elevates from 275 °C to 310 °C as M_{BDO} increases from 2000 tonnes to 18,000 tonnes. When M_{BDO} is 10,000 tonnes, the peak η_{eq} is 40.69% and the corresponding T_{9sv} is 295 °C. The thermodynamic parameters of each state point when $T_{9sv} =$ 310 °C are indexed in Table 4. Some points are missing because they are the same as those in Table 3.

The T_{9sv} corresponding to the maximum equivalent heat-to-power efficiency ($T_{9sv,eq}$) is higher than that corresponding to the maximum $\eta_{ORC-SRC}$. A design T_{9sv} lower than $T_{9sv,eq}$ can be recommended for the proposed system, because it can increase the efficiency in the normal condition and enlarge the electricity generation in the discharge mode.

Table 4
Thermodynamic parameters of each state point when $T_{9sv} = 310$ °C.

State point	Temperature (°C)	Pressure (MPa)	Enthalpy (kJ/kg)	Quality (%)
7	174.61	9.865	744.11	subcooled
8	212.38	9.865	911.21	subcooled
9	256.48	9.865	1117.10	subcooled
10	370	9.865	3002.70	superheated
11	273.34	4.54	2856.61	superheated
12	213.88	2.06	2724.67	95.86
13	213.88	2.06	2724.67	95.86
23	179.61	1.9982	761.84	subcooled
27	369.60	0.340	958.77	superheated
28	331.50	0.340	883.11	superheated
28_{sv}	320	0.340	861.10	100
29	320	0.340	651.26	–
30	320	0.340	601.40	0
31	321	0.959	602.44	subcooled
32	352.34	0.959	678.09	subcooled

5.4. Cost regarding the implementation of the ORC

The discharge period is selected as 7.5 h for both the ORC-SRC and the reference systems as mentioned in Section 5.2. For a simple comparison, the design steam evaporation temperatures are chosen as 310 °C in the economic analysis for the two systems, which are consistent with the operating conditions in mainstream PTC plants.

5.4.1. Cost of supplementary PTCs

The ORC-SRC increases the power output of the rated mode, but supplementary PTCs must be installed to concentrate solar energy in the daytime. The standard direct normal solar irradiance ($I_{DN,st}$) is 0.8 kW/m^2, and is perpendicular to the PTC aperture. The standard wind speed ($v_{w,st}$) is 5 m/s. The standard sunshine duration ($t_{s,st}$) is respectively 8.373, 7.649, 6.890, 6.392, 5.534 and 4.729 h for Phoenix, Lhasa, Sacramento, Cape Town, Canberra and Delingha according to the typical meteorological data [43]. The PTC inlet temperature is T_{32} for the ORC-SRC, while it is T_{LTT} for the reference system. The PTC efficiencies in the standard condition are respectively 72.284% and 72.964%. The required aperture area (A_{PTC}) and the extra PTC cost (C_{PTC}) are reported in Table 5. The least area is required in Phoenix as a result of the most abundant solar resource. $A_{PTC,ORC-SRC}$ is 8% more than $A_{PTC,ref}$ for each territory.

5.4.2. Cost of the IHX and other units

The investment of large heat exchangers is primarily determined by the heat transfer area and hence the total amount of required materials [44]. HTRI software ranks among state-of-the-art thermal process simulation and design software [45]. The required IHX area is estimated by HTRI software. A BFM type fixed tubesheet heat exchanger with double tubepasses and double shell side is adopted on account of its wide application, simple structure and small temperature drop (< 50 °C) of the shell side. The fluid with higher pressure is located in the tube side to reduce the IHX fabricating cost. Rod baffle is employed to reduce the flow resistance and the vibration in the shell. The tube pitch of 25 mm and tube outer diameter of 19 mm are adopted, which are common values in heat exchanger design.

It is difficult to accurately calculate the BDO mixture temperature in superheated (27 and 28) or subcooled (31 and 32) states according to the saturation pressure and enthalpy. Nevertheless, given the heat capacity and heat exchanger structure, the heat transfer coefficient is affected comprehensively by the temperatures, pressures and flow rates of both inlet and outlet, as well as the physical properties of fluids and the likelihood of phase change. It can be predicted that a deviation of several degrees Celsius on the inlet or outlet temperature has little effect on the design area of IHX. Take point 27 as an example, according to the conservation of energy, $Q = m_{ORC}(h_{27} - h_{28sv}) = m_{ORC} \cdot \overline{c_p} \cdot (T_{27} - T_{28sv})$. Where $\overline{c_p}$ is the average specific heat capacity and $\overline{c_p} = (c_{p27} + c_{p28sv})/2$. c_{p27} can be deduced approximately by linear interpolation based on h_{27} and the saturated vapor parameters, as there is little difference between

Table 5
Required PTC area and the additional cost in the rated mode.

Region	Required PTC area for the ORC-SRC ($\times 10^3$ m^2) ($A_{PTC,ORC-SRC}$)	Required PTC area for the indirect system ($\times 10^3$ m^2) ($A_{PTC,ref}$)	Additional cost of PTC ($\times 10^4$ $) ($C_{PTC}$)
Phoenix	227.993	211.035	288.281
Sacramento	277.036	256.430	350.293
Cape Town	298.648	276.435	377.620
Canberra	344.923	319.269	436.133
Lhasa	249.551	230.989	315.540
Delingha	403.676	373.652	510.422

Table 6
Design parameters of the IHX.

Process data	IHX
HTC at the shell side, kW/m^2·K	1.159
Internal diameter of the shell, mm	2200
Average velocity at the shell side, m/s	16.22
HTC at the tube side, kW/m^2·K	1.621
Length of the tube, m	13
Average velocity in the tube, m/s	0.87
Number of tubes	5423
Overall HTC, kW/m^2·K	0.500
Thermal load, MW	24.612
Average central spacing between baffles, mm	1000
Logarithmic mean temperature difference, °C	13.5
Area, m^2	4142.33
Over design, %	13.33

the specific heat capacity of saturated vapor state and superheated state when the enthalpy values are the same. It can be obtained $c_{p27} = 2.038$ kJ/(kg · K) and $T_{27} = 369.60$ °C when $T_{9sv} = 310$ °C. Analogously, $c_{p28} = 1.927$ kJ/(kg · K) and $T_{28} = 331.50$ °C.

The margin of IHX area is guaranteed to be above 10% and the process data is posted in Table 6. The scheme of the IHX is depicted in Fig. 14. The investments in IHX, ORC turbine, ORC generator and P4 are 151.305, 232.698, 33.995 and 20.675 × 10^4 $, respectively.

5.5. Equivalent payback period (EPP)

The computational procedure of *EPP* can be summarized in Fig. 15. Given the same design parameters of SRC, the rated generating power of SRC is the same for the proposed and reference systems. Meanwhile, the power outputs during discharge are the same for the two systems since the storage capacity is the same. But the initial investment for the proposed system is larger due to additional ORC equipment and PTCs, which results in higher normal efficiency and more power generation during the rated mode. The total power generation covers the nominal and discharge modes. The generated power is $W_{ORC-SRC}$ and W_{SRC} respectively for the proposed system, while it remains W_{SRC} during the two modes for the reference system. *EPP* is the ratio of the extra investment to the difference between the annual yield of power generation under the rated mode of the two systems, as indicated by Eq. (34).

Land cost is not considered as it is supposed to be lower than 8.0% of the solar field in a CSP system [11]. Annual electricity output in the rated mode and *EPP* are indexed in Table 7. The proposed system can generate an excess 1893.2–2208.5 × 10^4 kWh electricity (i.e., 348.349–406.364 × 10^4 $ revenue) per year at the additional cost of 726.954–949.095 × 10^4 $. The *EPPs* are less than 3 years in the six districts with rich solar radiation resource. The advantages of using the ORC as a top cycle of the SRC are evident. Notably, T_{9sv} of 310 °C is selected to better compare the proposed and conventional systems. The optimum T_{9sv} of the proposed system is expected to be below 310 °C to elevate the ORC-SRC efficiency and storage capacity. Therefore the *EPPs* will be further shortened if T_{9sv} is optimized.

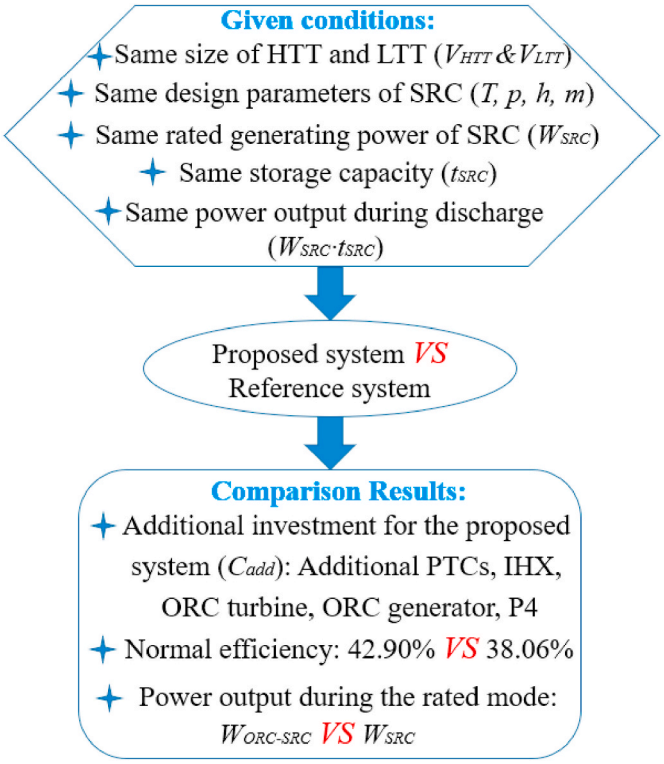

Fig. 15. Computational procedure of *EPP*.

Table 7
Annual electricity output in the rated mode and equivalent payback time.

Region	Annual electricity output for the ORC-SRC (× 10^4 kWh)	Annual electricity output for the indirect system (× 10^4 kWh)	Equivalent payback period (years)
Phoenix	14561.181	12404.214	1.832
Sacramento	13921.013	11873.135	2.094
Cape Town	14408.357	12294.115	2.098
Canberra	15118.424	12909.918	2.153
Lhasa	12813.475	10920.277	2.165
Delingha	13558.375	11632.303	2.678

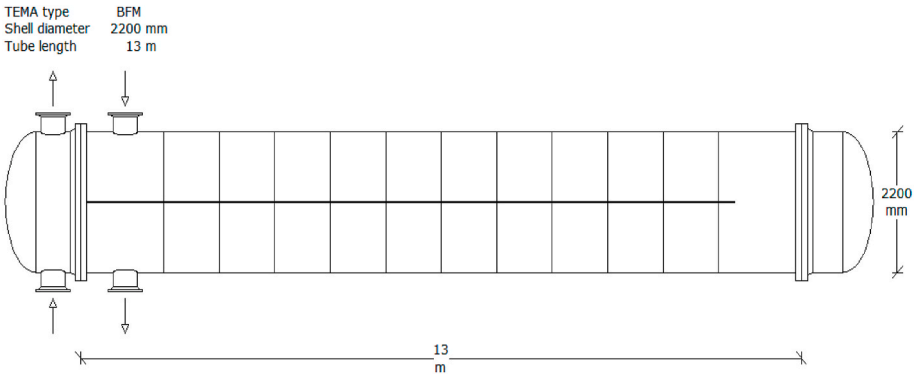

Fig. 14. Scheme of the IHX.

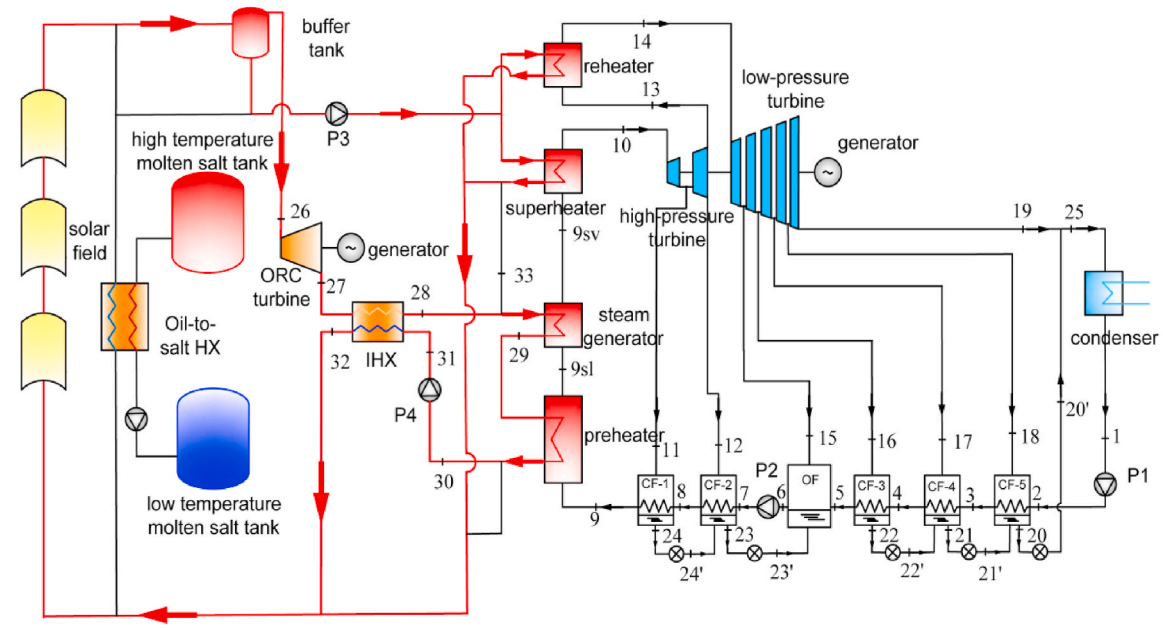

(a) Rated mode

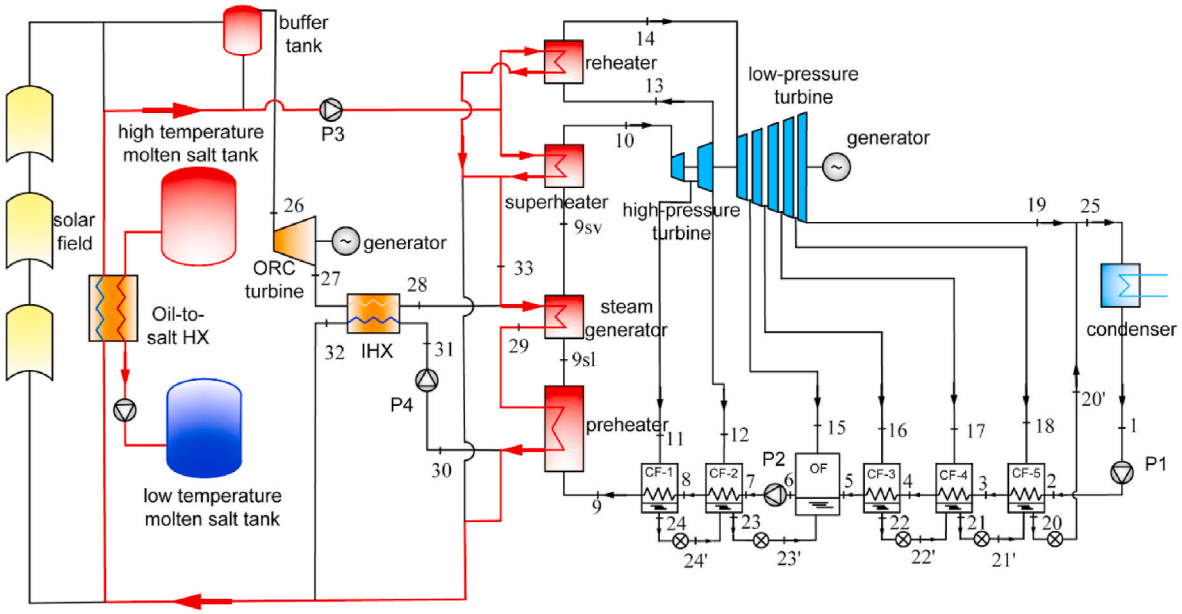

(b) Discharge mode

Fig. 16. Different modes of the modified system.

6. Additional aspects

Notably, the proposed ORC-SRC system is also applicable for thermal storage using molten salts by slight alteration. BDO mixture is still used for heat carrier and ORC fluid. An extra buffer tank is essential to store the BDO mixture. The two operating modes with molten salt storage are graphed in Fig. 16. The ORC-SRC efficiency is the same as that of the system in Fig. 2.

7. Conclusion

A novel DVG-CSP system combining cascade ORC-SRC with two-tank storage structure is presented. The ORC is on top of a conventional SRC and the high temperature vapor for the ORC is generated in the PTCs. The BDO mixture is employed as the heat carrier and storage medium, as well as the ORC working fluid. The system has two main operation modes. In the nominal mode, the vapor in the HTT drives the ORC turbine directly while the liquid, together with the exhaust heat released by the ORC, drives the SRC. In the discharge process, the liquid in the HTT flows into the LTT with a temperature drop of 81–121 °C, and the

bottom SRC is driven by the released sensible heat. Following conclusions are drawn.

1) There are good reasons for vapor generation of the BDO mixture in the solar field. The boiling/condensing heat transfer technology using the mixture up to 400 °C has reached a high level of maturity. The potential of the mixture in the waste heat-driven ORC systems has also been explored by both researchers and manufacturers, and no technical barriers have been identified in the literature. Contaminant prevention measures on the conventional oil-based CSP systems are still applicable for the proposed system, and a long BDO mixture lifespan is expected. No complicated control strategy is needed for vapor generation as the mixture can leave the solar field in either vapor or binary phase state and the power cycles in the charge and discharge processes are decoupled.
2) From the thermodynamic aspects, the proposed system not only elevates the average heat absorption temperature in the collectors (from 273 °C to 363 °C), but also guarantees stable power generation under fluctuating irradiation conditions. Moreover, it can increase the heat storage capacity considerably. The maximum temperature drop (from 390 °C to 269 °C) is larger than that of conventional dual-tank PTC-SRC systems (from 393 °C to 293 °C). It has an appreciably higher power efficiency (42.90% vs. 38.06%). The water evaporation temperature corresponding to the maximum cascade cycle efficiency is 50 °C lower than that in conventional PTC-SRC systems (260 °C vs. 310 °C). The equivalent payback period related to the implementation of ORC is generally within 3 years in the territories with abundant beam solar radiation resource. A shorter payback time is achievable via optimization of the water evaporation temperature.
3) Though dual-tank thermal oil storage is demonstrated in this paper, the improved efficiency, extended storage capacity and economic advantages are applicable when dual-tank molten salt storage is adopted.

Credit author statement

The contribution of each author is described as follows.

Pengcheng Li: Data curation, Investigation, Methodology, Formal analysis, Writing – original draft; Jing Ye: Resources, Software; Jing Li: Conceptualization, Formal analysis, Funding acquisition, Investigation, Methodology, Writing – review & editing; Yandong Wang: Resources, Software; Xiaobin Jiang: Formal analysis, Writing – review & editing; Tongle Qian: Writing – review & editing; Gang Pei: Writing – review & editing; Xunfen Liu: Writing – review & editing.

Declaration of competing interest

The authors declare that they have no known competing financial interests or personal relationships that could have appeared to influence the work reported in this paper.

Data availability

No data was used for the research described in the article.

Acknowledegment

This study was sponsored by National Natural Science Foundation of China (52206008), Fundamental Research Funds for the Central Universities of China (JZ2022HGTB0266), Science and Technology Major Project of Anhui Province (202003a05020025), DONGFANG ELECTRIC Dongfang Boiler Group CO., LTD., Postdoctoral Research Project of Sichuan Province.

References

[1] Hales D. Renewables 2020 global status report. Rep. Paris. 2020. p. 120–30. REN21, https://www.ren21.net/gsr-2020/chapters/chapter_03/chapter_03/#start-csp.
[2] Wang QL, Pei G, Yang HX. Techno-economic assessment of performance-enhanced parabolic trough receiver in concentrated solar power plants. Renew Energy 2021;167:629–43. https://www.sciencedirect.com/science/article/pii/S0960148112031884X.
[3] National Renewable Energy Laboratory (NREL) Project Listing. Parabolic Trough Proj. https://solarpaces.nrel.gov/by-technology/parabolic-trough. [Accessed 3 May 2022].
[4] Gonzalez-Gomez PA, Petrakopoulou F, Briongos JV, Santana D. Cost-based design optimization of the heat exchangers in a parabolic trough power plant. Energy 2017;123:314–25. https://doi.org/10.1016/j.energy.2017.02.002.
[5] https://productcatalog.eastman.com/tds/ProdDatasheet.aspx?product=71093459#_ga=2.232498588.2083174426.1648436972-368840163.1636878100. [Accessed 3 May 2022].
[6] Li J, Alvi JZ, Pei G, Ji J, Li PC, Fu HD, et al. Effect of working fluids on the performance of a novel direct vapor generation solar organic Rankine cycle system. Appl Therm Eng 2016;98:786. https://doi.org/10.1016/j.applthermaleng.2015.12.146. 97.
[7] Alvi JZ, Yu JH, Feng YQ, Asim M, Wang Q, Pei G. Performance assessment of direct vapor generation solar organic rankine cycle system coupled with heat storage. Sustainability 2022;14(22):15296. https://doi.org/10.3390/su142215296.
[8] Alvi JZ, Feng YQ, Wang Q, Imranb M, Pei G. Effect of working fluids on the performance of phase change material storage based direct vapor generation solar organic Rankine cycle system. Energy Rep 2021;7:348–61. https://doi.org/10.1016/j.egyr.2020.12.040.
[9] Alvi JZ, Feng YQ, Wang Q, Imranb M, Pei G. Effect of phase change materials on the performance of direct vapor generation solar organic Rankine cycle system. Energy 2021;223:120006. https://doi.org/10.1016/j.energy.2021.120006.
[10] Xu GQ, Song G, Zhu XX, Gao W, Li HW, Quan YK, et al. Performance evaluation of a direct vapor generation supercritical ORC system driven by linear Fresnel reflector solar concentrator. Appl Therm Eng 2015;80:196–204. https://doi.org/10.1016/j.applthermaleng.2014.12.071.
[11] Sinasac Z, Jianu OA. Parametric study on the exergetic and cyclic performance of a solar-powered organic Rankine cycle coupled with a thermal energy storage and complete flashing cycle. Sustain Energy Techn 2021;45:101172. https://doi.org/10.1016/j.seta.2021.101172.
[12] Casati E, Galli A, Colonna P. Thermal energy storage for solar-powered organic Rankine cycle engines. Sol Energy 2013;96:205–19. https://doi.org/10.1016/j.solener.2013.07.013.
[13] Casati E, Colonna P, Nannan NR. Supercritical ORC turbogenerators coupled with linear solar collectors. International solar energy society solar world congress. January 2011. https://doi.org/10.18086/swc.2011.25.06. At: Kassel, Germany.
[14] Casati E, Desideri A, Casella F, Colonna P. Preliminary assessment of a novel small CSP plant based on linear collectors, ORC and direct thermal storage. Proceedings solar PACES. 2012.
[15] Li J, Gao GT, Kutlu C, Liu KL, Pei G, Su YH, et al. A novel approach to thermal storage of direct steam generation solar power systems through two-step heat discharge. Appl Energy 2019;236:81–100. https://doi.org/10.1016/j.apenergy.2018.11.084.
[16] Vescovo R. High temperature organic rankine cycle (HT-ORC) for cogeneration of steam and power. AIP Conf Proc 2019:2191–20153. https://doi.org/10.1063/1.5138886.
[17] Vescovo R, Spagnoli E. High temperature ORC systems. Energy Proc 2017;129:82–9. https://doi.org/10.1016/j.egypro.2017.09.160.
[18] Bombarda P, Invernizzi C. Binary liquid metal-organic Rankine cycle for small power distributed high efficiency systems. Proc Inst Mech Eng, Part A: Journal of Power and Energy 2015;229:192–209. https://journals.sagepub.com/doi/full/10.1177/0957650914562094.
[19] Prieto C, Rodríguez A, Patiño D, Cabeza LF. Thermal energy storage evaluation in direct steam generation solar plants. Sol Energy 2018;159:501–9. https://doi.org/10.1016/j.solener.2017.11.006.
[20] González-Roubaud E, Pérez-Osorio D, Prieto C. Review of commercial thermal energy storage in concentrated solar power plants: steam vs. molten salts. Renew Sustain Energy Rev 2017;80:133–48. https://doi.org/10.1016/j.rser.2017.05.084.
[21] Eastman Corp; https://www.eastman.com/Literature_Center/T/TF9141.pdf [Accessed 3 May 2022].
[22] Padilla RV. Simplified methodology for designing parabolic trough solar power plants. University of South Florida, Graduate School Theses and Dissertations; 2011.
[23] Bronicki LY. The Ormat Rankine power unit. In: 7th Intersociety energy conversion engineering conference; 1972. p. 327–34. San Diego, USA, https://www.osti.gov/biblio/4467785.
[24] Turboden SpA. BRUNL, Cogenerative organic Rankine cycle system. International Publication Number: WO2017199170A1; 23 Nov 2017.
[25] Sampedro EO, Védie L. Wet to dry cycles for high temperature waste heat valorization using a diphenyl biphenyl oxide mixture. In: 6th international seminar on ORC power systems; October 11-13, 2021. Munich, Germany, https://mediatum.ub.tum.de/doc/1633030/1633030.pdf.
[26] Niggemann RE. Quarterly progress report no. 12 - organic rankine cycle technology program. Report, Sundstrand Corporation. Report No. SAN-651-96 Prepared under contract AT (04-3)-651 for the San Francisco Operations Office U.S. Atomic Energy Commission, 15 April 1969. https://www.osti.gov/servlets/purl/4774929.

[27] Anderson WG. Intermediate temperature fluids for heat pipes and loop heat pipes. In: 5th international energy conversion engineering conference and exhibit (IECEC); June 2007. p. 25–7. https://doi.org/10.2514/6.2007-4836. St. Louis, Missouri.
[28] Li PC, Cao Q, Li J, Wang Y, Pei G, Gao C, et al. Effect of regenerator on the direct steam generation solar power system characterized by prolonged thermal storage and stable power conversion. Renew Energy 2020;159:1099–116. https://doi.org/10.1016/j.renene.2020.06.037.
[29] Mohammadi K, McGowan JG. Thermodynamic analysis of hybrid cycles based on a regenerative steam Rankine cycle for cogeneration and trigeneration. Energy Convers Manag 2018;158:460–75. https://doi.org/10.1016/j.enconman.2017.12.080.
[30] Baumann K. Some recent developments in large steam turbine practice. Engineer 1921:435–58. https://doi.org/10.1049/JIEE-1.1921.0040. 111.
[31] Gao G, Li J, Li P, Cao J, Pei G, Dabwana YN, Su Y. Design of steam condensation temperature for an innovative solar thermal power generation system using cascade Rankine cycle and two-stage accumulators. Energy Convers Manag 2019;184:389–401. https://doi.org/10.1016/j.enconman.2019.01.067.
[32] THERMINOL® Heat Transfer Fluids by Eastman. https://www.therminol.com/. [Accessed 3 May 2022].
[33] Li J, Alvi JZ, Pei G, Su YH, Li PC, Gao GT, et al. Modelling of organic Rankine cycle efficiency with respect to the equivalent hot side temperature. Energy 2016;115:668–83. https://doi.org/10.1016/j.energy.2016.09.049.
[34] Li PC, Lin HW, Li J, Cao Q, Wang YD, Pei G, et al. Analysis of a direct vapor generation system using cascade steam-organic Rankine cycle and two-tank oil storage. Energy 2022;257:124776.
[35] Gao GT, Li J, Li PC, Yang HL, Pei G, Ji J, et al. Design and analysis of an innovative concentrated solar power system using cascade organic Rankine cycle and two-tank water/steam storage. Energy Convers Manag 2021;237:114108. https://doi.org/10.1016/j.enconman.2021.114108.
[36] Turton R, Bailie RC, Whiting WB, Shaeiwit JA, Bhattacharyya D. Analysis, synthesis, and design of chemical processes. Pearson Education Inc; 2009.
[37] Zhang C, Liu C, Wang SK, Xu XX, Li QB. Thermo-economic comparison of subcritical organic Rankine cycle based on different heat exchanger configurations. Energy 2017;123:728–41. https://doi.org/10.1016/j.energy.2017.01.132.
[38] Van LL, Abdelhamid K, Michel F, Sandrine PP. Thermodynamic and economic optimizations of a waste heat to power plant driven by a subcritical ORC (Organic Rankine Cycle) using pure or zeotropic working fluid. Energy 2014;78:622–38. https://doi.org/10.1016/j.energy.2014.10.051.
[39] Montes MJ, Abánades A, Martínez-Val JM, Valdés M. Solar multiple optimization for a solar-only thermal power plant, using oil as heat transfer fluid in the parabolic trough collectors. Sol Energy 2009;83:2165–76. https://doi.org/10.1016/j.solener.2009.08.010.
[40] Chacartegui R, Vigna L, Becerra JA, Verda V. Analysis of two heat storage integrations for an Organic Rankine Cycle Parabolic trough solar power plant. Energy Convers Manag 2016;125:353–67. https://doi.org/10.1016/j.enconman.2016.03.067.
[41] Delgado-Torres AM, García-Rodríguez L. Analysis and optimization of the low-temperature solar organic Rankine cycle (ORC). Energy Convers Manag 2010;51(12):2846–56. https://doi.org/10.1016/j.enconman.2010.06.022.
[42] Kurup P, Turchi CS. Parabolic trough collector cost update for the system advisor model (SAM). 2015. NREL/TP-6A20-65228.
[43] EnergyPlus. Weather data; 2017. https://energyplus.net/weather/. [Accessed 3 May 2022].
[44] Cataldo F, Mastrullo R, Mauro AW, Vanoli GP. Fluid selection of organic Rankine cycle for low-temperature waste heat recovery based on thermal optimization. Energy 2014;72:159–67. https://doi.org/10.1016/j.energy.2014.05.019.
[45] HTRI software. 2020. https://www.htri.net/. [Accessed 3 May 2022].

Nomenclature

A: aperture area, m^2
a: Baumann factor
C: cost, $/ coefficient
C_p: basic cost
F_p: pressure factor
h: enthalpy, kJ/kg
I: irradiance, W/m^2
K: coefficient
M: mass, kg
m: mass flow rate, kg/s
p: pressure, MPa
P: pump
P: price, $
Q: heat, kW
s: specific entropy, kJ/(kg·K)
S: entropy, kJ/K
T: temperature, °C
t: time duration, h
v: specific volume, m^3/kg
W: work, kW
w: power output by 1 kg BDO mixture, kWh/kg
Y: yield, $
y: wetness
ε: device efficiency, %
η: efficiency, %

Abbreviation

BDO: biphenyl/diphenyl oxide mixture
CEPCI: Chemical Engineering Plant Cost Index
CF: closed feedwater
CSP: concentrated solar power
DSG: direct steam generation
DVG: direct vapor generation
EPP: equivalent payback period
HP: high-pressure
HTC: heat transfer coefficient
HTT: high temperature tank
IHX: internal heat exchanger
LP: low-pressure
LTT: low temperature tank
ORC: organic Rankine cycle
ORC-SRC: organic-steam Rankine cycle
OF: open feedwater
PTC: parabolic trough collector
SRC: steam Rankine cycle

Subscript

0,1,2 …: number
a: ambient
add: additional
av: average
b: basic
BM: bare module
col: collectors
d: discharge
DN: direct normal
e: electricity
EHST: equivalent hot side *temperature:*
eq: equivalent
g: generator
HT: high-pressure turbine
in: inlet
LT: low-pressure turbine
min: minimum
out: outlet
OT: ORC turbine
P: Pump
rated: rated mode
ref: reference
s: isentropic
s h: superheated
sl: saturated liquid
st: standard
sv: saturated vapor